JOURNAL OF GEOPHYSICAL RESEARCH, VOL. 104, NO. B10, PAGES 23,141–23,153, OCTOBER 10, 1999

Numerical simulations of depth-dependent anisotropy and frequency-dependent wave propagation effects

Georg Rümpker

GeoForschungsZentrum Potsdam, Potsdam, Germany

Andréa Tommasi[1] and J.-Michael Kendall

School of Earth Sciences, University of Leeds, Leeds, England, United Kingdom

Abstract. A numerical investigation of the effects of shear wave splitting for vertical propagation in a smoothly varying anisotropic medium is presented. Through forward modeling, we predict the olivine lattice preferred orientation (LPO) developed in the oceanic upper mantle in response to the absolute plate motion (APM). We consider the effect of a change in APM similar to the one that presumably caused the kink in the Emperor-Hawaii seamount island chain in the north Pacific. This results in an oblique orientation between lithospheric and asthenospheric anisotropy. Numerical simulations of shear wave propagation are used to estimate the characteristics of shear-wave splitting. Ray theory does not account for coupling between shear waves in the depth-dependent anisotropic medium due to the implicit assumption of high frequency. A forward propagator technique for calculating waveforms and splitting parameters is used to assess frequency-dependent effects. The results show that ray theory is valid for estimating the splitting only for frequencies above 1 Hz. At frequencies more realistic for *SKS* propagation, apparent splitting parameters exhibit a $\pi/2$ dependence on the incoming shear wave polarization (back azimuth). For certain back azimuth ranges, shear wave splitting is very frequency dependent with apparent delay times ranging from 1 to 4 s and apparent fast polarization directions changing rapidly by up to 80°. Thus stacking of shear wave splitting measurements for largely different initial polarizations and frequencies should be avoided. Depth-dependent anisotropy implies that shear wave splitting analyses will be sensitive to filtering. Anisotropic depth variations cannot be resolved unambiguously from splitting observations at relatively long periods (>5 s). It is not possible, for instance, to discriminate between smooth and abrupt transitions separating the anisotropic regions. Shorter-period waveforms provide further information on the fine structure of anisotropic depth variations. A comparison between splitting calculations and observations from Hawaii suggests a divergent past APM direction or may indicate an alternative mechanism responsible for the lithospheric anisotropy.

1. Introduction

The seismic anisotropy exhibited by upper mantle rocks is primarily a function of the intrinsic anisotropy and of the degree of orientation of the constituent crystals. Evidence of flow and deformation causing such petrofabric ordering comes from a wide range of studies. Refraction studies have first shown evidence of azimuthal anisotropy within the oceanic upper mantle which, *Hess* [1964] interpreted as an expression of olivine crystal alignment frozen into the lithosphere at the time of formation at a spreading center. Support for this interpretation has come from petrofabric analyses in upper-mantle xenoliths [*Mainprice and Silver*, 1993; *Nicolas and Christensen*, 1987], as well as in peridotites from ophiolites [*Christensen*, 1966, 1978; *Christensen and Crosson*, 1968; *Peselnik and Nicolas*, 1978] and orogenic massifs [*Avé-Lallemant and Carter*, 1970; *Nicolas et al.*, 1971; *Nicolas and Christensen*, 1987]. The alignment of olivine crystals in response to simple shear [*Zhang and Karato*, 1995] and axial compression [*Nico-*

[1]Now at Laboratoire de Tectonophysique, Université Montpellier II, Montpellier, France.

Paper number 1999JB900203.
0148-0227/99/1999JB900203$09.00

las et al., 1973] was also observed in laboratory studies of deformation in peridotites. Finally, numerical simulation of flow-induced textures allows the prediction of olivine lattice preferred orientations and seismic anisotropy that may develop in the upper mantle in response to a given flow field [*Chastel et al.*, 1993; *Blackman et al.*, 1996; *Tommasi et al.*, 1996].

Perhaps the most diagnostic feature of anisotropy is the observation of two roughly orthogonally polarized shear waves propagating with different velocities. Analyses of splitting in core phases like *SKS* are now routine. The increasing ease of deploying seismic arrays of broadband three-component seismometers enables regional studies which offer insights into tectonic processes within the mantle. In continental domains, fast shear waves are usually polarized parallel to the regional structural trend, suggesting a pervasive deformation of the lithospheric mantle during orogenic events [*Silver*, 1996; *Vauchez et al.*, 1998]. Nevertheless, there are still many assumptions which go into the interpretations of these results. In this paper we explore the link between the upper mantle structure and seismic anisotropy observations. We are specifically interested in the frequency-dependent nature of shear wave splitting measurements and its relationship to variations in anisotropy with depth. Through a forward numerical model linking thermomechanical and texture simulations, we predict the deformation and resulting olivine lattice preferred orientations developed in response to a given flow process [*Tommasi*, 1998]. Splitting parameters are estimated from elasticity models derived from the lattice preferred orientation (LPO) predictions. The situation considered is the evolution of anisotropy in the oceanic upper mantle. Oceanic lithosphere is formed at a spreading center, thickening with distance from the ridge by progressive cooling of asthenospheric material [*Blackman et al.*, 1996; *Tommasi et al.*, 1996]. Olivine LPO develops in the asthenosphere in response to the absolute plate motion (APM), and as the plate cools, it is progressively frozen in the lithosphere. We consider the effects of wave propagation in two cases: a constant APM direction and a change in APM direction. The latter results in an oblique olivine LPO in the lithosphere and asthenosphere. We use both the forward propagator approach of *Rümpker and Silver* [1998] and its ray theoretical approximation to predict *SKS* splitting through these models. Ray theoretical methods implicitly assume that we are dealing with relatively high frequencies which may not be appropriate for modeling teleseismic signals. To address this issue and assess the validity of ray theoretical calculations, we compare the results for the two methods. Furthermore, the possibility to discriminate between different models of depth-varying anisotropy is investigated in some detail. Our results apply to regions which can be characterized by layers with a more or less horizontal a axis direction. Further complications arise in regions with dipping layers [e.g., *Fouch and Fischer*, 1998] and general variations of anisotropy [G. Rümpker and P. G. Silver, manuscript in preparation, 1999].

2. Depth-Dependent Seismic Anisotropy in Ocean Basins

We use the forward modeling approach of *Tommasi* [1998] to simulate the development of depth-dependent lattice preferred orientations and hence seismic anisotropy in the oceanic upper mantle. The finite strain field associated with the asthenospheric deformation by resistive drag beneath an oceanic plate is calculated using a vertical plane strain finite element model [*Tommasi et al.*, 1996] in which the oceanic plate and underlying upper mantle are simulated by a homogeneous material able to deform by dislocation creep following a dry dunite constitutive relation (Table 1). The upper boundary of the model is submitted to a constant velocity of 6 cm yr^{-1}, whereas the lower boundary (at 500 km depth) is kept fixed. Upper and lower boundaries have fixed temperatures of 273 and 1773 K, respectively, and a null heat flow is prescribed at the lateral boundaries. The initial temperature field consists of a 2 m.y. old oceanic plate geotherm calculated using a

Table 1. Thermomechanical Model Parameters

Parameter	Value
Volumic mass ρ, kg m^{-3}	3350
Heat capacity C, W kg^{-1} K^{-1}	1100
Heat conductivity for lithosphere (k_L), W m^{-1} K^{-1}	3.5
Heat conductivity for asthenosphere (k_A), W m^{-1} K^{-1}	4.67
Material constant A,* Pa^{-n} s^{-1}	2.42×10^{-16}
Activation energy E,* kJ mol^{-1}	540
Activation volume V,* m^3 mol^{-1}	1.7×10^{-5}
Stress exponent n*	3.5

*Parameters defining the relationship between strain rate $\dot{\epsilon}$ and deviatoric stress σ for a dry dunite as well as its temperature (T) and pressure (P) dependencies [*Karato and Wu*, 1993]: $\dot{\epsilon} = A \exp[-(E + PV)/RT]\,\sigma^n$.

half-space cooling model and an adiabatic gradient in the sublithospheric mantle. Convective heat transfer in the sublithospheric mantle is simulated through an enhanced thermal conductivity (Table 1).

Strain is localized in a horizontal shear zone several tens of kilometers wide between an almost rigid mechanical lithosphere and a mildly deformed upper mantle. Shear strain accumulates progressively with plate displacement. As the plate cools, the upper part of the deformed layer freezes, and the shear zone migrates toward deeper levels. The fabric responsible for the measured anisotropy is therefore contained in two distinct layers: a frozen lithospheric layer and an asthenospheric layer that records the current plate motion. The thickness of the deformed layers depends not only on the time elapsed (or displacement) but also on the velocity of the plate. Plates with different velocities have different shear strain rate profiles: for a similar displacement, faster plates accumulate larger shear strains over thinner layers [*Tommasi et al.*, 1996]. We use the anisotropic viscoplastic self-consistent (VPSC) approach developed by *Lebensohn and Tomé* [1993] to calculate the olivine LPO evolution due to this deformation. An olivine polycrystal is associated with each nodal point of a vertical profile in the central domain of the finite element model. The deformation of the polycrystal is described by the velocity gradient and finite strain tensors that characterize the flow at this point in the thermomechanical model. Through an interaction equation that relates local stresses and strain rates (s, $\dot{e}$) to the macroscopic stress and strain rate (σ, $\dot{\epsilon}$), the VPSC model predicts the evolution of the aggregate yield strength, the activity of slip systems, and LPO development. At the grain scale, deformation is accommodated by dislocation glide on crystallographic systems (Table 2); other deformation mechanisms, like dynamic recrystallization, are not taken into account. This is justified when considering that naturally or experimentally deformed peridotites (which are recrystallized) and the predictions of the polycrystal plasticity models (that do not simulate recrystallization) show essentially the same textures [e.g., A. Tommasi et al., Viscoplastic self-consistent and equilibrium-based modeling of olivine lattice preferred orientations. 1. Implications for upper mantle seismic anisotropy, submitted to *Journal of Geophysical Research*, 1999]. Model aggregates are composed of 400 grains. Before deformation they display random lattice preferred orientations, and grains are supposed to be equiaxed.

Table 2. Slip Systems Data in VPSC Models

Slip System	CRSS*	Stress Exponent n
(010)[100]	1	3.5
(001)[100]	1	3.5
(010)[001]	2	3.5
(100)[001]	3	3.5
{011}[100]	4	3.5
{031}[100]	4	3.5
{110}[001]	6	3.5

VPSC, viscoplastic self-consistent.

*The normalized (relative to (010)[100]) critical resolved shear stresses (CRSS) indicate the relative strengths of the various slip systems considered in the models.

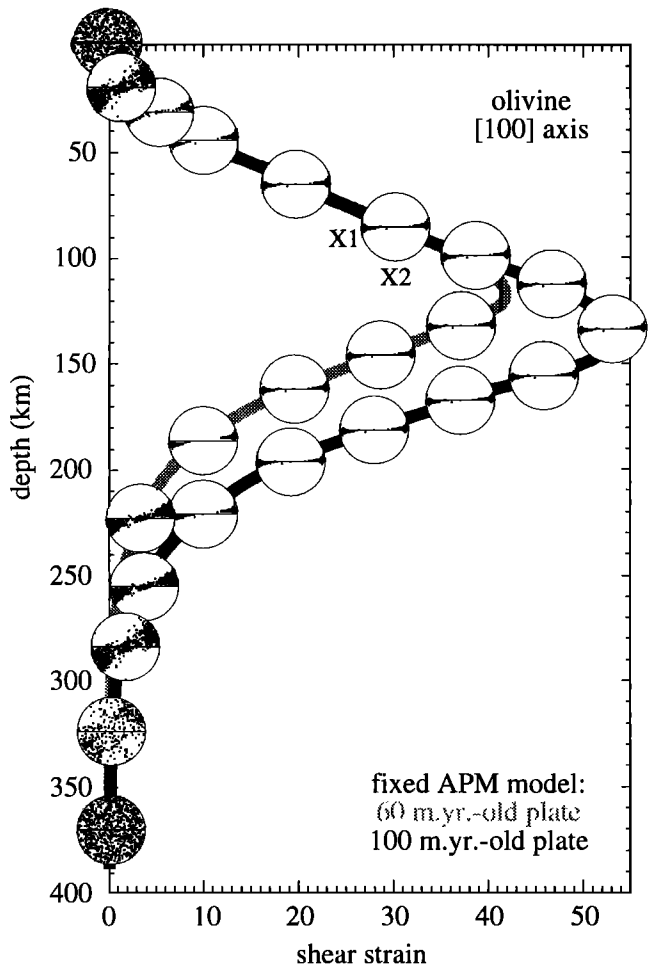

Figure 1. Shear strain profiles and olivine lattice preferred orientations (only the [100] axis is represented) as functions of depth for models M1 (100 m.y. old plate) and M2 (60 m.y. old plate). X1 is the absolute plate motion (APM) direction and X2 is the vertical direction.

The shear strain profile and corresponding [100] axis preferred orientations for a 60 m.y. old plate and a 100 m.y. old plate with fixed APMs (N70°W, Models M1 and M2) are presented in Figure 1. Clear LPO patterns are already developed at shear strains as low as 0.5, and most of the deformed layer displays [100] nearly parallel to the flow direction (i.e., the APM). The effect of a change in the APM on the upper mantle fabrics is investigated through a model in which the plate moved toward N10°W with a velocity of 6 cm yr^{-1} for 60 m.y. and then changed instantaneously to a N70°W direction during the last 40 m.y. (i.e., an APM evolution similar to the one suggested for the northern Pacific by

the Emperor-Hawaii hotspot track). Figure 2 shows the variation with depth of olivine LPO in this model (M3). The uppermost mantle displays frozen lattice preferred orientations related to the old APM. The deeper levels display LPO related to the current plate motion. Between these two layers there is a thick transitional layer in which a slow rotation of the LPO between the two orientations occurs. Reorientation of LPO in this model is slow, because such a large APM change (60°) places the olivine [001] axes close to the new shear direction, leading to deformation through simultaneous slip on (010)[001] and (0̄10)[100]. Thus even instantaneous changes in APM result in a gradational reorientation of olivine LPO with depth, the thickness of the transitional layer depending on the angle between the two plate motion directions. Finally, in order to compare the effects of a smooth LPO reorientation and an abrupt LPO reorientation in the seismic response, in model M4, the continuous rotation of LPO of model M3 is replaced by a sharp discontinuity at a depth of 110 km. If single-crystal elastic stiffness coefficients [*Kumazawa and Anderson*, 1969], the volume fraction of the different mineral phases composing an aggregate, and their crystallographic preferred orientation are known the elastic properties of the aggregate may be calculated using a Voigt-Reuss-Hill average of the stiffnesses (C_{ijkl}) over all crystal orientations [*Mainprice*, 1990]. Seismic properties calculated for modeled olivine polycrystals agree well with those calculated using olivine LPO measured in naturally deformed peridotites [*Tommasi*, 1998]. However, the composition of our model polycrystals (100% olivine) leads to an overestimation of the seismic anisotropy. Thus, in the following, elastic constants are calculated for aggregates composed of 70% olivine (with LPO taken from our models) and 30% enstatite which display a typical high-temperature deformation LPO measured in a naturally deformed harzburgite from the Oman ophiolite.

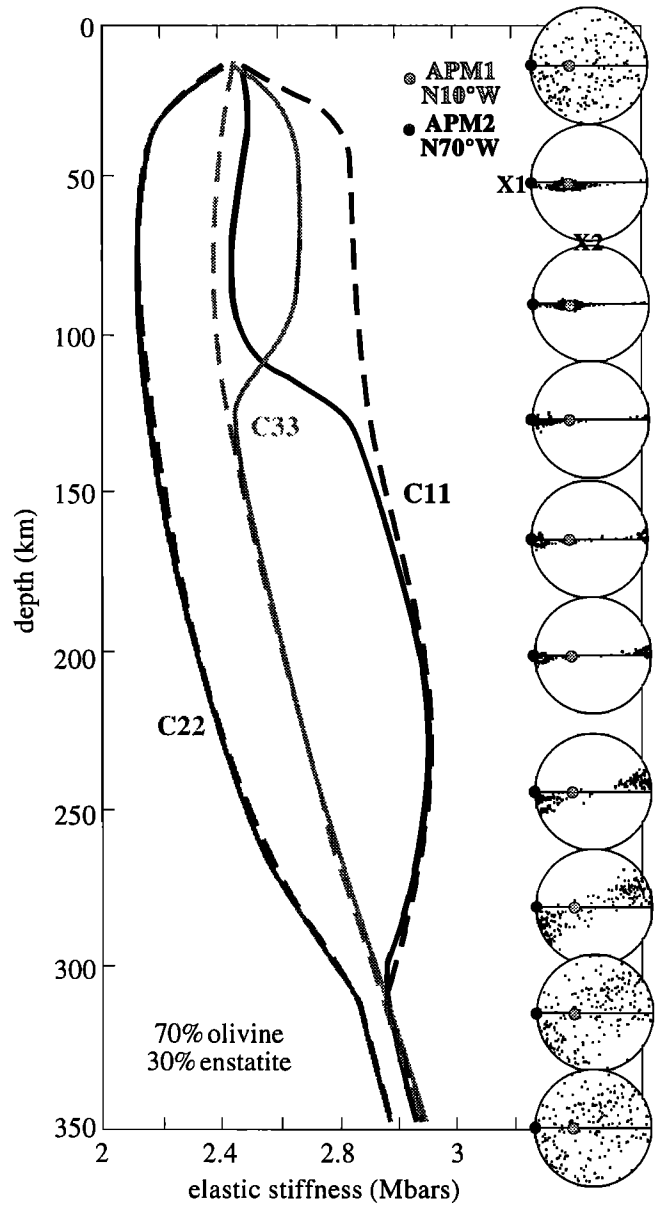

Figure 2. (left) The C11, C22, and C33 components of the elastic stiffness tensor for models M3 (solid lines) and M1 (dashed lines).(right) Olivine lattice preferred orientation (LPO) (only the [100] axis is represented) as a function of depth for model M3 (100 m.y. old plate with an APM change at 40 Ma). X1 is the present APM direction, and X2 is the vertical direction.

Figure 3 shows the depth dependence of the (horizontal) fast shear wave polarization direction ("fast axis") and accumulated delay time for shear waves traveling vertically in the four upper mantle models. The polarization directions have been calculated from the Christoffel equation using the elastic constants obtained from the 70% olivine, 30% enstatite model aggregates. The accumulated delay time Δt is defined as the depth integral over incremental delay times δt, given by

$$\Delta t(z) = \int_0^z \delta t = \int_0^z [p_s(\xi) - p_f(\xi)] d\xi \qquad (1)$$

where p_s and p_f are the vertical slowness components of the slow and fast shear waves and $d\xi$ is the depth increment.

Fast axis directions in the upper parts of both M1 and M2 are close to the plate motion direction (N70°W, i.e., -70°). Deviations from this direction in the lower part of M2 correspond to relatively weak anisotropy, as is shown by the slow increase in accumulated delay time in this depth range. For most of the model, however, the accumulated delay time increases uniformly and reaches values of Δt =2.71 s for M1 and Δt =1.85 s for M2. These relatively large values are maximum estimates [e.g., *Tommasi et al.*, 1996]. A uniform increase in Δt indicates that the strength of the anisotropy, which reaches values of about 4.6%, varies little over the corresponding depth interval. This is in agreement with the observation that seismic anisotropy for both P and S waves displays a very weak dependence on LPO intensity and hence on finite strain in high-strain do-

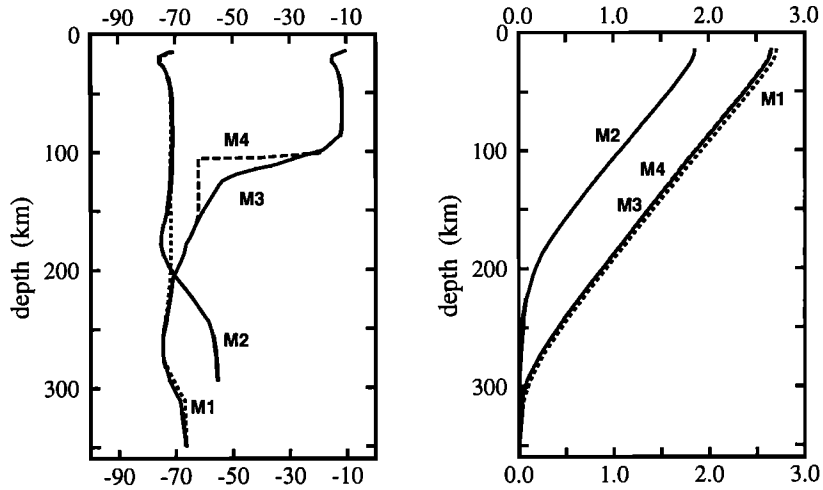

Figure 3. (left) The fast polarization direction (degrees) and (right) the accumulated delay time (seconds). Both are shown as functions of depth for upper mantle models M1 – M4. The strength of the anisotropy reaches approximately 4.6 %.

mains (shear strains higher than 5 [*Tommasi*, 1998]). Fast axis directions for M3 and M4 are close to N10°W (-10°) in the upper regions and close to N70°W (-70°) in the lower regions of the models. For M3, fast axis directions change smoothly between depths of 90 and 130 km, whereas M4 exhibits a discontinuity at a depth of about 110 km. Accumulated delay times for both models are essentially the same at all depths and (for the most part) increase uniformly to reach values of Δt =2.65 s.

3. Forward Propagator Approach and Frequency-Dependent Effects

Recently, *Rümpker and Silver* [1998] studied shear wave splitting effects for vertical propagation in multilayered and smoothly varying anisotropic media. Seismograms were calculated using a forward propagator matrix approach, which neglects effects of back scattering but accounts for frequency-dependent forward scattering (coupling) between the two shear waves. For smoothly varying anisotropic media the forward propagator and full finite difference methods lead to virtually identical shear wave splitting. The former, however, is much less computationally expensive and thus applicable to inversions. The most elementary medium considered by Rümpker and Silver can be described by three parameters: the fast axis directions at the top (ϕ_t) and base (ϕ_b) of the anisotropic region and the total (accumulated) delay time (Δt). Calculated waveforms exhibit a strong frequency dependence. At relatively long periods ($T/\Delta t > 5$) the particle motion is elliptical and varies systematically with the polarization of the incident wave. At a fixed initial polarization these results can be described in terms of an apparent fast polarization direction ϕ_a and an apparent delay time δt_a. At shorter periods ($T/\Delta t < 1$) the seismogram for a smoothly varying medium consists of two arrivals, polarized parallel to the fast and slow axis directions at the top of the anisotropic region. The smoothly varying media considered by Rümpker and Silver are characterized by uniformly changing fast axis directions and constant delay time increments. Our models (M1 – M4) exhibit more complicated depth variations of anisotropy as is shown in Figure 3. However, the forward propagator method still applies and can be used to simulate vertical wave propagation and to study the frequency dependence of splitting parameters and waveforms. The results also provide a test for ray theoretical predictions since the method is independent of assumptions concerning the frequency content of the incident wave field.

3.1. Forward Propagator Versus Ray Theory

Anisotropic ray theory is valid under the assumption that apart from effects at discontinuities, the two shear waves propagate independently. For vertical wave propagation in a smoothly varying region, the ray theory seismogram depends on the fast axis orientations at the base and top. The fast axis at the base relative to the initial polarization determines the relative amplitudes of the fast and slow shear waves, whereas the fast axis orientation at the top determines the final polarization directions. Intermediate smooth variations of the fast axis have no effect on the final seismogram. The delay time between fast and slow wave accumulates along the ray path and depends on the strength of the anisotropy within the region traversed. The forward propagator, on the other hand, accounts for frequency-dependent coupling between the shear waves while the polarizations vary along the ray paths. The method provides an effective way to account for coupling in multilay-

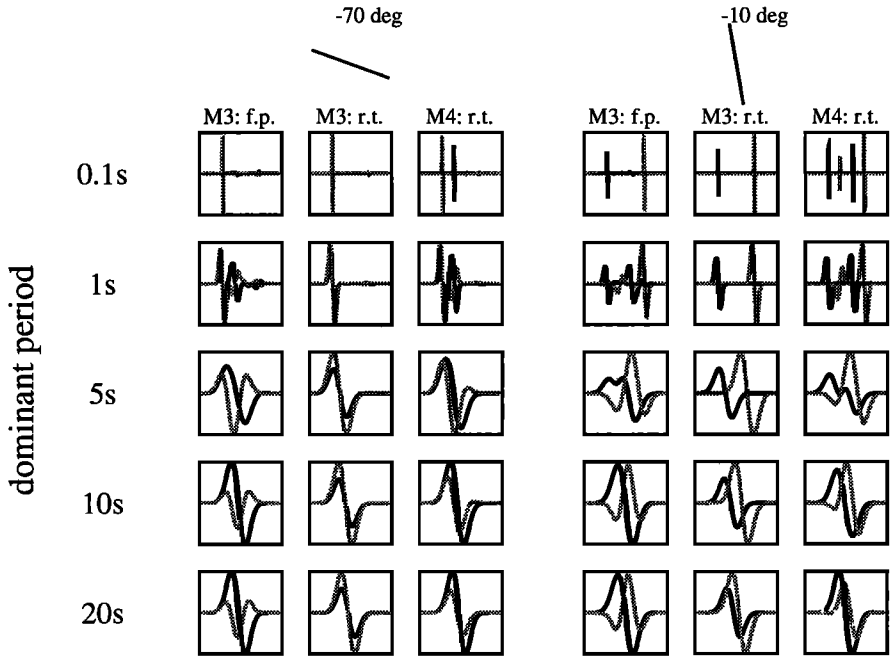

Figure 4. Radial (solid) and transverse (shaded) displacement components as functions of dominant period and initial polarization (degrees). For M3, waveforms have been calculated using both the forward propagator (f.p.) and ray theory (r.t.). For M4, ray theoretical results are shown. Note that the timescale changes with dominant period.

ered anisotropic regions; smooth variations are approximated by arbitrarily fine layering.

Can ray theory be used to calculate seismograms for media with depth-dependent variations of anisotropy? To investigate this, we calculated waveforms for M3 using both the forward propagator method and its ray theoretical (high frequency) approximation. In addition, ray theory is applied to model M4, thus taking into account the wave interactions at a single discontinuity. The waveforms are given in Figure 4 for dominant periods T between 0.1 and 20 s and for initial polarizations of -70° and -10°. The long-period ray theory seismograms have been obtained by filtering of the short-period results. In our examples the initial wavelet is given by the derivative of a Gaussian-shaped pulse. For M3 the results agree only at periods $T < 1$ s. In this case, the seismograms exhibit a dominant fast arrival since the fast axis at the base is parallel to the initial polarization (-70°). For an initial polarization of -10° the seismogram exhibits a fast arrival and a slow arrival, separated by the accumulated delay time Δt. In both cases, the fast arrival is polarized parallel to the fast axis direction at the top of the anisotropic medium. For M4 there are up to two additional intermediate arrivals due to the discontinuity at depth 110 km.

At $T = 1$ s the forward propagator seismogram exhibits intermediate arrivals similar to those obtained for M4 (using ray theory). The amplitudes, however, are markedly different. For longer periods, individual arrivals interfere and cannot be distinguished. Only for the forward propagator results are the radial and transverse displacement components characteristic of (long period) shear wave splitting: The transverse component is the approximate time derivative of the radial component, and the corresponding particle motion (not shown here) is elliptical with a main axis more or less parallel to the initial polarization direction. The ray theory particle motions do not show these characteristics. We conclude that ray theoretical calculations cannot be extrapolated to model waveforms and splitting parameters in strongly depth-dependent (or inhomogeneous) media at periods relevant to *SKS* observations. In the following sections, the forward propagator method is used to study characteristics of shear wave splitting for waves propagating vertically in upper mantle models M1 – M4.

3.2. Apparent Splitting Parameters

For an anisotropic medium with N distinct layers, the complete seismogram consists of contributions from 2^N split shear waves. At sufficiently low frequencies, individual arrivals overlap, and apparent splitting parameters can be obtained under the assumption of a single anisotropic layer, when in reality the medium exhibits variations of anisotropy with depth. Frequency-dependent apparent splitting parameters for depth-dependent media can be calculated analytically [*Rümpker and Silver*, 1998]. The frequency dependence is related to the coupling between the two shear waves in inho-

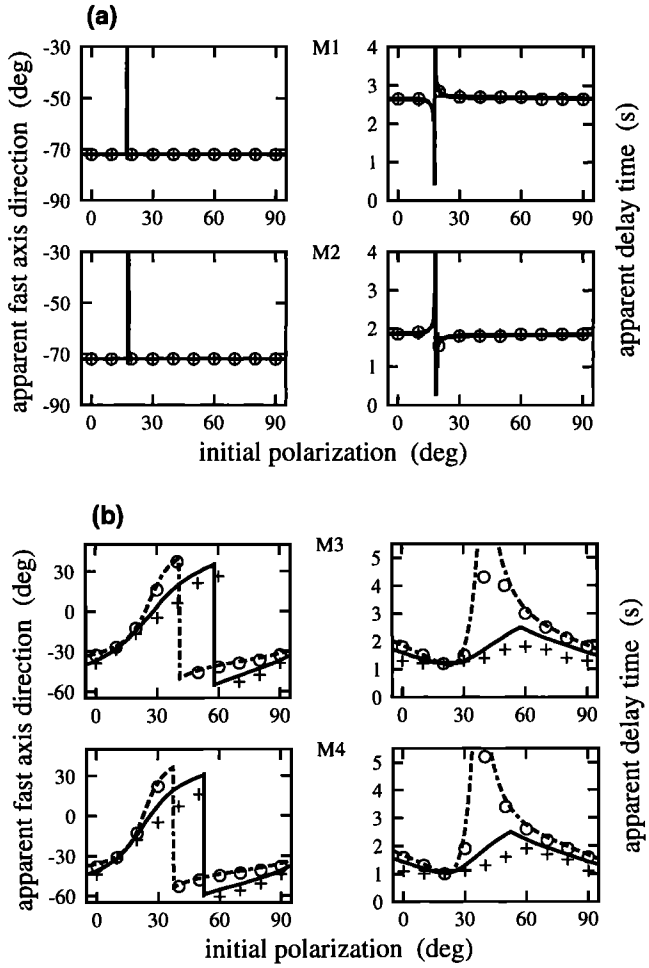

Figure 5. (a) Apparent splitting parameters as functions of initial polarization for M1 and M2. (b) The same as in Figure 5a except for M3 and M4. Calculated splitting parameters for periods of 5 s (solid lines) and 20 s (dashed lines) are compared with measurements on synthetic waveforms at dominant periods of 5 s (crosses) and 20 s (circles). In view of the periodicity, apparent splitting parameters are shown for initial polarizations between 0° and 90°.

mogeneous anisotropic media [*Chapman and Shearer*, 1989; G. Rümpker and P. G. Silver, manuscript in preparation, 1999]. The calculated apparent splitting parameters agree well with results obtained from synthetic seismograms using the method of *Silver and Chan* [1991]. Figure 5 shows apparent splitting parameters for models M1 – M4 as functions of initial polarization, which have been obtained using both methods. Examples are given for periods $T = 20$ s and $T = 5$ s. The calculated curves are compared with measurements on waveforms of the same (dominant) period. For M1 and M2 the frequency dependence of apparent splitting parameters is negligible, and the curves cannot be distinguished in this representation. The apparent splitting parameters are independent of initial polarization except near about 20° where fast axis direction and delay time are indeterminate. This is related to initial polarizations which are either perpendicular or parallel to the dominant fast axis direction in the medium (about -70°), such that splitting cannot be observed (sometimes called "null" directions). For these models the splitting can effectively be described by a single homogeneous anisotropic layer. The (apparent) one-layer splitting parameters are $\phi_a = -72°$, $\delta t_a = 2.7$ s (M1), and $\delta t_a = 1.8$ s (M2), respectively. Parameter ϕ_a agrees with the average fast axis direction in the medium, and values for δt_a agree with the maximum accumulated delay time Δt for the models (Figure 3). Calculated and measured apparent splitting parameters are in excellent agreement. In principle, ray theoretical calculations can give satisfactory results for M1 and M2, which are effectively one-layer models for which scattering effects and the frequency dependence of splitting parameters can be neglected.

On the other hand, the apparent splitting parameters for M3 and M4 exhibit considerable variation with frequency and initial polarization, which is caused by the strong variations in the orientation of the fast axis with depth [*Rümpker and Silver*, 1998]. The results for M3 and M4 are similar, although the discontinuity in ϕ_a and the maximum in δt_a occur at slightly larger initial polarization for M4. The calculated and measured apparent fast axis directions exhibit variations between -50° and 40° at both periods; however, the discontinuity in ϕ_a moves to larger initial polarizations at shorter periods. The maximum apparent delay time is reduced significantly. Consequently, at relatively short periods, apparent delay times vary less rapidly as a function of initial polarization.

Rümpker and Silver [1998] have derived analytical expressions of splitting parameters which are valid for simple three-parameter models with uniformly varying fast axis directions and constant delay time increments. In the low-frequency limit, "jumps" of ϕ_a occur whenever the initial polarization $\phi_{\hat{\mathbf{p}}}$ is equal to the arithmetic mean of the fast axis directions at the top and base of the anisotropic region:

$$\phi_{\hat{\mathbf{p}}} = \frac{\phi_t + \phi_b}{2} \tag{2}$$

For this direction the apparent delay time is proportional to the dominant period of the incident wave:

$$\delta t_a \sim T \tag{3}$$

Assuming $\phi_t = -10°$ and $\phi_b = -70°$, we expect jumps to occur at $\phi_{\hat{\mathbf{p}}} = -40°$ (+50°). For M3 with $T = 20$ s a jump occurs near +40°, which is relatively close to our estimate. For this initial polarization, values of δt_a change by about a factor 4 for periods between $T = 5$ s and $T = 20$ s, which is in agreement with equation (3). Rümpker and Silver show that the transverse displacement component is relatively weak for initial polarizations given by equation (2) and that splitting

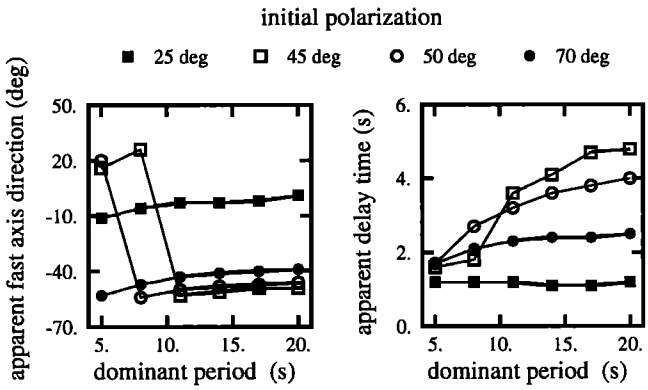

Figure 6. Apparent splitting parameters as functions of the dominant period for M3. The results have been obtained from measurements on synthetic waveforms.

will be difficult to observe. However, our measurements on theoretical seismograms (Figure 5) indicate that the splitting can still be resolved.

For M3 the most rapid variations with frequency occur near an initial polarization of 45°, where the apparent fast axis direction changes by about 70° and the (measured) apparent delay time changes by almost 4 s for the two periods shown. Generally, measurements and calculations are in good agreement; somewhat larger differences occur at shorter periods. Note that the calculated curves are valid for a single period, whereas the measurements are based on complete waveforms. Apparent splitting parameters at even longer periods are not significantly different from the result at $T = 20$ s. On the other hand, apparent splitting parameters for periods $T < 5$ s become meaningless, as individual arrivals separate and results can not be described by only two parameters.

Figure 6 shows the frequency dependence of the apparent splitting parameters for M3 in greater detail. The results have been obtained from measurements on the synthetic waveforms, which are less sensitive to small changes in dominant period than directly calculated splitting parameters are. A pronounced frequency dependence is shown for initial polarizations of 45° and 50°. For these polarizations the apparent fast axis direction can undergo rapid changes by up to 80° at periods between 5 and 12 s. This corresponds to a relatively strong increase in apparent delay times. The frequency variations are relatively weak for initial polarizations of 25° and 70°; the former exhibits a slight decrease in apparent delay time near dominant periods of 15 s.

3.3. Waveforms

We now consider a wider frequency range and show waveforms (radial and transverse displacement components) with dominant periods between 10 and 0.1 s (Figure 7). At long periods ($T = 10$ s) the transverse component varies rapidly as a function of initial polarization, whereas the radial component changes only slightly. To first order, the waveform of the transverse component in all models is given by the derivative of the radial component. This is a characteristic of "classical" shear wave splitting due to a single anisotropic layer with a well-defined fast axis. At shorter periods ($T = 1$ s), seismograms for M1 and M2 exhibit a fast arrival and a slow arrival, each containing radial and transverse components; the corresponding amplitudes strongly depend on the initial polarization. The pulses are separated by the accumulated delay time Δt characteristic for each model. For M1 and M2, with $\phi_{\hat{\mathbf{p}}} = -70°$, the transverse component is relatively weak since $\phi_{\hat{\mathbf{p}}}$ is close to the fast-axis in the medium. For M3 and M4, with $\phi_{\hat{\mathbf{p}}} = -70°$, the splitting is dominated by the effect of the upper anisotropic region. (Note the small-amplitude slow arrivals.) The corresponding apparent splitting parameters (Figure 5b) for $\phi_{\hat{\mathbf{p}}} = -70° + 90° = 20°$ are characterized by a minimum

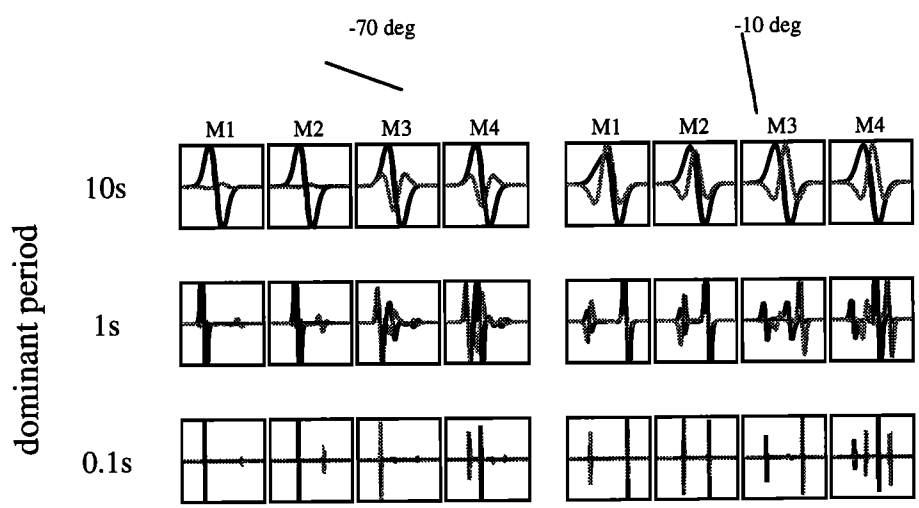

Figure 7. Radial (solid) and transverse (shaded) displacement components as functions of dominant period and initial polarization (degress) for models M1 – M4.

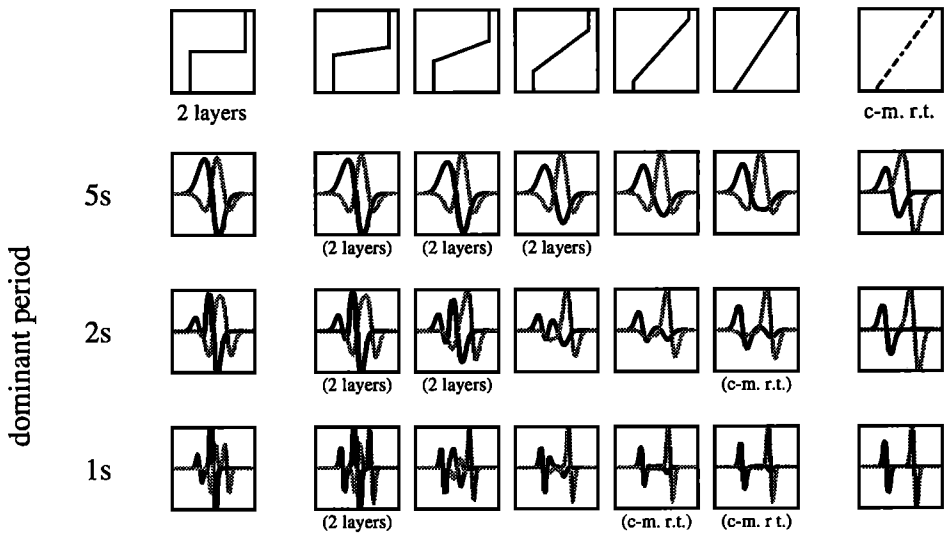

Figure 8. Radial (solid) and transverse (shaded) displacement components as functions of dominant period. The top row indicates variations of fast axis directions with depth. (left) Waveforms for two anisotropic layers with fast axis directions of -70° and -10°. Forward propagator and ray theory give identical results in this case. (right) Ray theory waveforms obtained under the assumption that the fast polarization direction varies continuously (continuous medium ray theory (c-m. r.t.)).

in δt_a and ϕ_a close to the dominant fast axis in the upper regions of the models. The seismograms for M3 and M4 are more complicated and exhibit additional intermediate arrivals, which for M3 become negligibly small at $T = 0.1$ s. There are, however, up to four arrivals for M4. This is generally a characteristic of models with two distinct anisotropic layers [*Silver and Savage*, 1994]. The intermediate arrivals are caused by the discontinuity in anisotropic properties at a depth of 110 km, where additional splitting occurs. A comparison with M3 shows that frequency-dependent amplitude variations of the intermediate arrivals are related to the sharpness of the transition between upper and lower anisotropic regions.

3.4. Effects of a Smooth Transition

In Figure 8 we study effects of the transition between anisotropic regions in greater detail. Our "starting model" consists of two anisotropic layers with fast axis directions $\phi_1 = -70°$ (lower layer), $\phi_2 = -10°$ (upper layer), and $\delta t_1 = \delta t_2 = 1$ s. Waveforms are shown at three periods between 5 and 1 s for an initial polarization of -40°. The results have been calculated using the forward propagator approach. For the two-layer case, however, the same results can be obtained from ray theory, provided that the effects of the interface are taken into account explicitly. For additional models the interface between the layers is replaced by a transition zone, where that fast axis changes linearly with depth. In our examples, the "thickness" (DT) of the transition zone varies between 0.2 and 2 s. Furthermore, waveforms are shown for the high-frequency approximation of the forward propagator which is equivalent to ray theory in a continuously varying medium. In this case, the waveforms only depend on the orientation of the symmetry axis at the top and base of the anisotropic region.

In Figure 8 we have indicated the results that more or less agree with the two-layer case, on one hand, or with continuous medium ray theory, on the other. We find that for (approximately) $T/DT > 5$ the smooth transition cannot be resolved, and a two-layer model can be used to calculate the waveforms. A characteristic of the corresponding seismogram is the large-amplitude intermediate arrivals at shorter periods. For $T/DT < 1$ the seismogram exhibits dominant fast and slow arrivals and continuous medium ray theory is appropriate. At intermediate periods the smooth transition causes low-amplitude intermediate arrivals, and waveforms cannot be assigned to either of the two limiting cases. Applying these results to M3, we obtain approximately $DT = 0.4$ s (Figure 3), which leads to the estimate that waveform calculations for M3 and M4 give similar results if $T > 2$ s, whereas continuous medium ray theory is appropriate for $T < 0.2$ s.

3.5. Ambiguity of Observations at Long Periods

Recent observations of azimuthal variations of splitting parameters [*Vinnik et al.*, 1994; *Özalaybey and Savage*, 1994; *Brechner et al.*, 1998] have been interpreted in terms of two anisotropic layers which can be characterized by four parameters. *Rümpker and Silver* [1998] have shown that the observed variations in those cases can also be explained in terms of three-parameter mod-

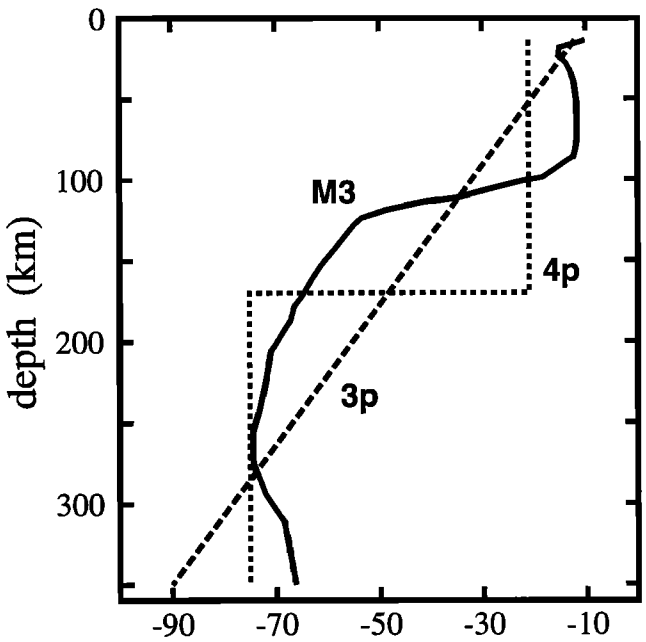

Figure 9. The fast polarization direction (degrees) as function of depth for M3 in comparison with those for a three-parameter model with uniformly varying fast axis and for a four-parameter model with two distinct anisotropic layers.

els with smooth variations of anisotropy, provided the deformation history at a given station does not pose any further constraints on the inversion. Here we assume depth variations of anisotropy as given by M3 and perform an inversion of (long period) splitting parameters in terms of simple three- and four-parameter models. Do the results reflect the given variations of anisotropy with depth?

With apparent splitting parameters for M3 as a reference (at a period of 10 s), we performed an inversion using a grid search algorithm [e.g., *Özalaybey and Savage*, 1994]. For the three parameters of the smoothly varying model, we obtain $\phi_b = -90°$, $\phi_t = -12°$, and $\Delta t = 2.2$ s. The best fit two-layer model is given by $\phi_1 = -75°$ and $\delta t_1 = 1.5$ s (lower layer) and $\phi_2 = -21°$ and $\delta t_2 = 1.3$ s (upper layer). The corresponding variations of fast axis direction with depth are given in Figure 9. In the smoothly varying case, ϕ_t is close to the fast axes in the upper part of M3, whereas ϕ_b deviates by about 20° from the dominant fast axis orientation in the lower part of M3. The range of fast axis directions covered by this model is thus slightly larger than that for M3. In the two-layer case, ϕ_1 and ϕ_2 closely resemble the main fast axis directions in the upper and lower regions of M3. However, the boundary between the two layers occurs at a depth about 50 km below the transition zone of M3. Note, however, that the strength of the anisotropy, as measured by the delay time increment over a depth interval, is assumed to be constant for the two simple models on which the inversion is based.

Figure 10 shows seismograms for the three models starting at a dominant period of $T = 20$ s, where the waveforms are virtually indistinguishable. At $T = 5$ s some differences occur and become more pronounced as the dominant period decreases. In the two-layer case, intermediate arrivals remain strong at shorter periods, whereas for M3, amplitudes decrease further. There

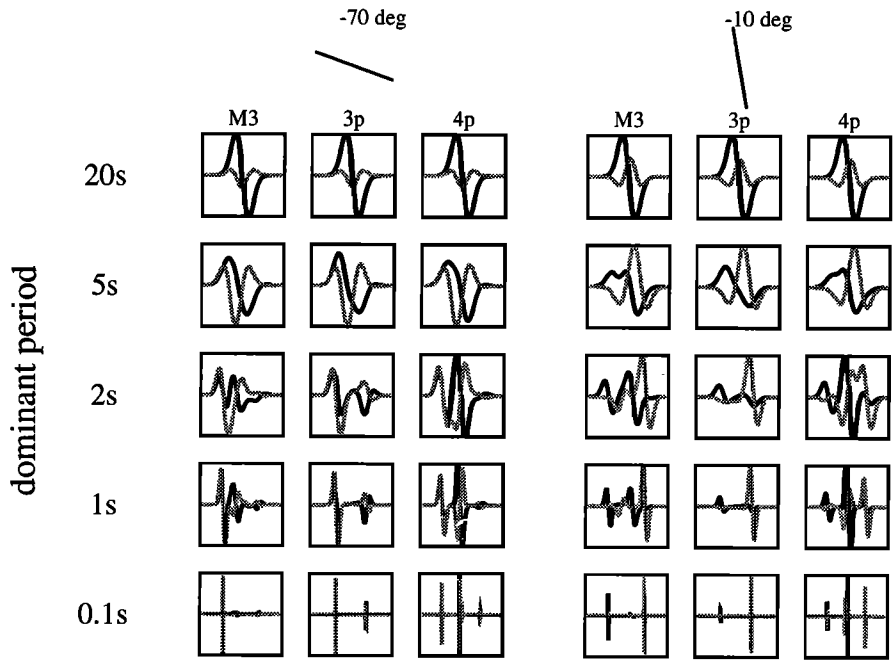

Figure 10. Radial (solid) and transverse (shaded) displacement components as functions of dominant period and initial polarization (degrees) for M3 in comparison with waveforms for the three- and four-parameter models.

are apparently no intermediate arrivals for the three-parameter model. At $T = 0.1$ s both the smoothly varying model and M3 exhibit only two (main) arrivals. However, delay times and amplitudes differ; the latter only depend on the axis directions at the base and top of the medium.

3.6. Comparison With Shear Wave Splitting Data in Hawaii

A wide range of shear wave splitting measurements has been presented for the Geoscope KIP station (Oahu, Hawaii). While the stacked solution of *Wolfe and Silver* [1998] displays an E-W (-87°) fast shear wave polarization and a delay time of 0.9 s, individual measurements by *Ansel and Nataf* [1989] as well as the stacked solution of *Vinnik et al.* [1989] point to a NE fast shear wave polarization (44°, 1.0 s; 26°, 1.4 s; and 45°, 1.5 s). Recent individual measurements by *Barruol and Hoffmann* [1999] also point to a NE fast shear wave polarization (45°) and a delay time close to 1 s.

Neither of these fast shear wave polarizations are observed for the model M3, which simulates an APM change similar to the one responsible for the Emperor - Hawaii island chain bend. From our modeling we would expect fast polarization observations in the range between -50° and 30°, depending on the polarization of the incoming wave. A similar discrepancy between data and modeling has already been noted by *Tommasi* [1998]. The present calculations confirm that it is not due to a possible inadequacy of the two-layer model used in that study, with the possible explanation that the Emperor chain trend may not record the northern Pacific APM before 43 Ma (see *Tommasi* [1998] for a more detailed discussion).

Wolfe and Silver [1998] further suggest that KIP data may be fit by a two-layer model with a present-day APM component in the lower layer (-58°, 0.45 s) and a larger fossil component, parallel to the fracture zones (spreading direction) in the upper layer (75°, 0.75 s). Apparent fast polarizations (not shown) for this model exhibit only minor variations, and are close to $\phi_a = 80°$, over a range of initial polarizations between 30° and 90°. The fast shear wave polarization in the uppermost layer is in agreement with P_n data in this region [*Morris et al.*, 1969]. However, this model implies that LPO formed at the spreading center is preserved in an approximately 90-km-thick layer, which suffers no further deformation in spite of the asthenospheric temperatures in its lower part.

The *SKS* splitting observations of *Barruol and Hoffmann* [1999] indicate the lowest apparent delay times for initial polarizations between -80° and -50°. If we assume that the lowermost anisotropy results from resistive drag in response to the present-day APM (close to -70°), shear waves with these initial polarizations are weakly sensitive to the deep anisotropy (see section 3.3). Their splitting records essentially the lithospheric mantle structure. Under this assumption, the observations of Barruol and Hoffmann indicate a NE fast polarization with delay times of 0.75-1.0 s in the lithospheric part of the mantle. However, this fast polarization in the upper layer disagrees with the P_n anisotropy measured north of Hawaii [*Morris et al.*, 1969].

Assuming that the fast axis orientation in the asthenosphere (lower layer) corresponds to the present-day APM direction, we performed a grid search to determine the fast direction in the upper layer (of a two-layer model) that approximately fits the observed fast polarizations of 45°. Setting $\phi_1 = -70°$ and $\delta t_1 = 1.5$ s (lower layer), we found $\phi_2 = +39°$ and $\delta t_2 = 1.2$ s (upper layer). The corresponding splitting parameters exhibit a range of fast polarization direction between about 0° and 80°, depending on the initial polarization. This is more compatible with previous observations. However, an APM direction of +39° (or -141°) in the northern Pacific before 43 Ma is difficult to explain in view of present geodynamic models for the Pacific plate evolution.

4. Discussion and Conclusions

Fluid-dynamical models with fixed APM exhibit only minor depth variations of anisotropy. Consequently, the shear wave splitting can essentially be described by a single homogeneous anisotropic layer. In this case, the frequency dependence of the splitting parameters is negligible, and ray theoretical calculations can be extrapolated to longer periods. On the other hand, changes in the direction of plate motion can induce significant variation of anisotropy with depth, which leads to a pronounced frequency dependence of waveforms and splitting parameters. In these situations, (continuous medium) ray theoretical calculations of shear wave splitting are inappropriate at periods larger than about 1 s and lead to false predictions. More complete methods, such as the forward propagator method, are necessary to study waveform effects for a wider frequency range.

At relatively long periods ($T/\Delta t > 5$), seismograms can be characterized by two apparent splitting parameters which exhibit a $\pi/2$ periodicity as functions of initial polarization. For $T = 20$ s, calculations predict variations of apparent fast axis direction between about -50° and 30° with delay times varying between 1 and 4 s, depending on the polarization (back-azimuth) of the incident wave front. At $T = 5$ s, calculated apparent delay times (for all initial polarizations) are systematically lower than the integrated delay time of the input model. Yet direct measurement on synthetic waveforms shows that the calculated delay time variations are usually somewhat overestimated. In addition, for similar anisotropic layer thicknesses a medium with a vertically varying anisotropy will display lower apparent delay times than a uniform anisotropic medium will for most of the initial polarization range. Observations of abruptly changing fast axis directions usually coincide with a relatively weak transverse component. How-

ever, results from measurements near those directions should not automatically be dismissed as "outliers" since they might provide important clues on depth-dependent structures. Important information about the depth variations also comes from analyzing the minimum of the apparent delay times as a function of initial polarization. The smallest delay time is independent of frequency for periods between 5 and 20 s. Under the assumption of two dominant fast axis orientations in the medium, it corresponds to a wave with initial polarization $\phi_{\bar{b}}$ approximately parallel or perpendicular to the fast axis in the lower part (ϕ_b), and it may therefore be used to constrain ϕ_b (from the initial polarization), as well as ϕ_t (from the apparent polarization).

Analysis of Hawaii data in the light of these results shows that observed polarization directions do not agree with apparent polarizations calculated for model M3, which simulates an APM change similar to the one thought to be responsible for the Emperor-Hawaii island chain bend. This supports previous suggestions [*Norton*, 1995; *Tarduno and Cottrell*, 1997; *Tommasi*, 1998] that the Emperor chain trend may not record the northern Pacific APM before 43 Ma. Recent data [*Barruol and Hoffmann*, 1999; *Wolfe and Silver*, 1998] may indeed indicate depth-dependent anisotropy with the asthenosphere displaying an APM-related fabric and either an ENE [*Wolfe and Silver*, 1998] or a NE [*Barruol and Hoffmann*, 1999] fast axis orientation in the uppermost mantle.

Inverting for the fast polarization in the upper (second) layer while keeping the fast polarization in the lower layer fixed at $\phi_1 = -70°$ leads to a value $\phi_2 = 39°$. The corresponding splitting parameters for this two-layer model exhibit a range of fast polarizations which is similar to the observed values. However, an APM direction of +39° (or -141°) in the northern Pacific before 43 Ma, to our knowledge, is not supported by the paleomagnetic data or other constraints.

For depth-dependent anisotropy, splitting measurements should yield variable fast polarizations as a function of initial polarization and frequency. These polarizations have not been observed conclusively at KIP. This is possibly due to the limited range of initial polarizations (back azimuths) for which splitting has been observed. In future studies the stacking of individual splitting measurements for largely different initial polarizations or dominant periods should be avoided.

Frequency variations of apparent splitting parameters are most obvious for initial polarizations close to discontinuities of the apparent fast axis orientation. Near these initial polarizations, small variations in frequency can cause changes in apparent fast axis orientation by up to 80°, while the apparent delay times increase by up to about 4 s for dominant periods between 5 and 20 s (M3). A similar frequency dependence of apparent delay times has recently been observed by *Marson-Pidgeon and Savage* [1997] and was attributed to oriented heterogeneities.

The nature of anisotropic depth variations cannot be resolved unambiguously from splitting observations at relatively long periods, which might be considered typical for SKS. For example, splitting parameters for model M3 can be explained by relatively simple depth variations of anisotropy which can be described in terms of only three or four parameters. Inversions based on these models can still give meaningful variations of fast axis directions that closely resemble those in the medium (M3). Furthermore, smooth transitions between anisotropic regions cannot be discriminated from discontinuities at relatively long periods ($T/\Delta t > 5$).

The determination of apparent splitting parameters breaks down at shorter periods when individual arrivals separate and the seismogram cannot be characterized by only two parameters (at periods $T < 5$ s in our case). However, short-period waveforms provide further information on the fine structure of anisotropic depth variations. Amplitudes of intermediate arrivals decrease with frequency for media with smooth variations of fast axis orientation. The amplitudes remain strong for media with discontinuities. These effects can potentially be observed using broadband *SKS* data. A systematic study of variations of waveforms and splitting parameters from individual events in different frequency bands is currently underway.

Acknowledgments. We are grateful to Karen Fischer, Michel Granet, and Klaus Mosegaard for constructive reviews.

References

Ansel, V., and H. C. Nataf, Anisotropy beneath 9 stations of the Geoscope broadband network as deduced from shear-wave splitting, *Geophys. Res. Lett.*, *16*, 409-412, 1989.

Avé-Lallemant, H. G., and N. L. Carter, Synthetic recrystallization of olivine and modes of flow in the upper mantle, *Geol. Soc. Am. Bull.*, *81*, 2003-2020, 1970.

Barruol, G., and R. Hoffmann, Upper mantle anisotropy beneath the Geoscope stations, *J. Geophys. Res.*, *104*, 10,757-10,773, 1999.

Blackman, D. K., J.-M. Kendall, P. R. Dawson, H.-R. Wenk, D. Boyce, and J. Phipps-Morgan, Teleseismic imaging of subaxial flow at mid-ocean ridges: Travel-time effects of anisotropic mineral texture in the mantle, *Geophys. J. Int.*, *127*, 415-426, 1996.

Brechner, S., K. Klinge, F. Krüger, and T. Plenefisch, Back-azimuthal variations of splitting parameters of teleseismic SKS-phases observed at the broadband stations in Germany, *Pure Appl. Geophys.*, *151*, 305-331, 1998.

Chapman, C. H., and P. M. Shearer, Ray tracing in azimuthally anisotropic media II. Quasi–shear wave coupling, *Geophys. J. Int.*, *96*, 65-83, 1989.

Chastel, Y. B., P. R. Dawson, H.-R. Wenk, and K. Bennet, Anisotropic convection with implications for the upper mantle, *J. Geophys. Res.*, *98*, 17,757-17,771, 1993.

Christensen, N. I., Elasticity of ultrabasic rocks, *J. Geophys. Res.*, *71*, 5921-5931, 1966.

Christensen, N. I., Ophiolites, seismic velocities and oceanic crustal structure, *Tectonophysics*, *47*, 131-157, 1978.

Christensen, N. I., and R. S. Crosson, Seismic anisotropy in the upper mantle, *Tectonophysics*, *6*, 93-107, 1968.

Fouch, M. J., and K. M. Fischer, Shear wave anisotropy in

the Mariana subduction zone, *Geophys. Res. Lett.*, *25*, 1221-1224, 1998.

Hess, H. H., Seismic anisotropy in the uppermost mantle under oceans, *Nature*, *203*, 629-631, 1964.

Karato, S., and P. Wu, Rheology of the upper mantle: A synthesis, *Science*, *260*, 771-778, 1993.

Kumazawa, M., and O. L. Anderson, Elastic moduli, pressure derivatives, and temperature derivatives of single-crystal olivine and single-crystal forsterite, *J. Geophys. Res.*, *74*, 5961-5972, 1969.

Lebensohn, R. A., and C. N. Tomé, A self-consistent anisotropic approach for the simulation of plastic deformation and texture development of polycrystals: Application to zirconion alloys, *Acta Metall. Mater.*, *41*, 2611-2624, 1993.

Mainprice, D., A FORTRAN program to calculate seismic anisotropy from the lattice preferred orientation of minerals, *Comput. & Geosci.*, *16*, 385-393, 1990.

Mainprice, D., and P. G. Silver, Interpretation of SKS-waves using samples from the subcontinental lithosphere, *Phys. Earth Planet. Inter.*, *78*, 257-280, 1993.

Marson-Pidgeon, K., and M. K. Savage, Frequency-dependent anisotropy in Wellington, New Zealand, *Geophys. Res. Lett.*, *24*, 3297-3300, 1997.

Morris, G. B., R. W. Raitt, and G. G. Shor Jr., Velocity anisotropy and delay-time maps of the mantle near Hawaii, *J. Geophys. Res.*, *74*, 4300-4316, 1969.

Nicolas, A., and N. I. Christensen, Formation of anisotropy in upper mantle peridotites - A Review, in Composition, Structure and Dynamics of the Lithosphere-Asthenosphere System, *Geodyn. Ser., vol. 16*, edited by K. Fuchs and C. Froidevaux, pp. 111-123, AGU Washington D.C., 1987.

Nicolas, A., J. L. Bouchez, F. Boudier, and J. C. Mercier, Textures, structures and fabrics due to solid state flow in some European lherzolites, *Tectonophysics*, *12*, 55-86, 1971.

Nicolas, A., F. Boudier, and A. M. Boullier, Mechanism of flow in naturally and experimentally deformed peridotites, *Am. J. Sci.*, *273*, 853-876, 1973.

Norton, I. O., Plate motions in the North Pacific: The 43 Ma nonevent, *Tectonics*, *14*, 1080-1094, 1995.

Özalaybey, S., and M. K. Savage, Double-layer anisotropy resolved from S phases, *Geophys. J. Int.*, *117*, 653-664, 1994.

Peselnik, L., and A. Nicolas, Seismic anisotropy in an ophiolite peridotite: Application to oceanic upper mantle, *J. Geophys. Res.*, *83*, 1227-1235, 1978.

Rümpker, G., and P. G. Silver, Apparent shear-wave splitting parameters in the presence of vertically-varying anisotropy, *Geophys. J. Int.*, *135*, 790-800, 1998.

Silver, P. G., Seismic anisotropy beneath the continents: Probing the depths of geology, *Annu. Rev. Earth Planet. Sci.*, *24*, 385-432, 1996.

Silver, P. G., and W. W. Chan, Shear wave splitting and subcontinental mantle deformation, *J. Geophys. Res.*, *96*, 16,429-16,454, 1991.

Silver, P. G., and M. K. Savage, The interpretation of shear-wave splitting parameters in the presence of two anisotropic layers, *Geophys. J. Int.*, *119*, 949-963, 1994.

Tarduno, J. A., and R. D. Cottrell, Paleomagnetic evidence for motion of the Hawaiien hotspot during the formation of the Emperor seamounts, *Earth Planet. Sci. Lett.*, *153*, 171-180, 1997.

Tommasi, A., Forward modeling of the development of seismic anisotropy in the upper mantle, *Earth Planet. Sci. Lett.*, *160*, 1-13, 1998.

Tommasi, A., A. Vauchez, and R. Russo, Seismic anisotropy in ocean basins: Resistive drag of sublithospheric mantle?, *Geophys. Res. Lett.*, *23*, 2991-2994, 1996.

Vauchez, A., A. Tommasi, and G. Barruol, Rheological heterogeneity, mechanical anisotropy and deformation of the continental lithosphere, *Tectonophysics*, *296*, 61-86, 1998.

Vinnik, L. P., V. Farra, and B. Romanowicz, Azimuthal anisotropy in the Earth from observations of SKS at Geoscope and NARS broadband stations, *Bull. Seismol. Soc. Am.*, *79*, 1542-1558, 1989.

Vinnik, L. P., V. G. Krishna, R. Kind, P. Bormann, and K. Stammler, Shear wave splitting in the records of the German Regional Seismic Network, *Geophys. Res. Lett.*, *21*, 457-460, 1994.

Wolfe, C. J., and P. G. Silver, Seismic anisotropy of the oceanic upper mantle: Shear wave splitting methodologies and observations, *J. Geophys. Res.*, *103*, 749-771, 1998.

Zhang, S., and S. Karato, Lattice preferred orientation of olivine aggregates in simple shear, *Nature*, *375*, 774-777, 1995.

J.-M. Kendall, School of Earth Sciences, University of Leeds, Leeds LS2 9JT, England, U.K. (M.Kendall@earth.leeds.ac.uk)

G. Rümpker, GeoForschungsZentrum Potsdam, Telegrafenberg, 14473 Potsdam, Germany. (rumpker@gfz-potsdam.de)

A. Tommasi, Laboratoire de Tectonophysique, Université Montpellier II, Place Eugne Batillon, 34095 Montpellier cedex 5, France. (deia@dstu.univ-montp2.fr)

(Received November 17, 1998; revised May 25, 1999; accepted June 8, 1999.)